frontiers in Chemistry

ORIGINAL RESEARCH
published: 04 September 2019
doi: 10.3389/fchem.2019.00595

Facile Synthesis of Novel $V_{0.13}Mo_{0.87}O_{2.935}$ Nanowires With High-Rate Supercapacitive Performance

Haishun Jiang[1], Wenjing Sun[1], Wenyao Li[1], Zhe Wang[1], Xiying Zhou[1]*, Zexing Wu[2] and Jinbo Bai[3]**

[1] School of Material Engineering, Shanghai University of Engineering Science, Shanghai, China, [2] College of Chemistry and Molecular Engineering, Qingdao University of Science and Technology, Qingdao, China, [3] Laboratoire Mécanique des Sols, Structures et Matériaux, CNRS UMR 8579, Ecole Centrale Supelec, Université Paris Saclay, Châtenay-Malabry, France

Binary metal oxides composed of molybdenum–vanadium oxides are promising candidates for supercapacitors. Here, we report the synthesis of one-dimensional $V_{0.13}Mo_{0.87}O_{2.935}$ nanowires through a facile one-step hydrothermal method. This nanowire presented a high specific capacitance of 394.6 F g^{-1} (1 mV s^{-1}) as an electrode applied to the supercapacitor. Importantly, this electrode showed a perfect rate capability of 91.5% (2 to 10 A g^{-1}) and a continuous verified outstanding cyclic voltammetry of 97.6% after 10,000 cycles. These superior electrochemical properties make the synthesized $V_{0.13}Mo_{0.87}O_{2.935}$ nanowires a prospective candidate for high-performance supercapacitors.

Keywords: molybdenum–vanadium oxides, nanowires, hydrothermal, high rate, supercapacitors

OPEN ACCESS

Edited by:
Elizabeth J. Podlaha, Clarkson University, United States

Reviewed by:
Dipankar Roy, Clarkson University, United States
John Zhanhu Guo, University of Tennessee, Knoxville, United States

****Correspondence:***
Wenyao Li
liwenyao314@gmail.com
Xiying Zhou
zhouxiying@sues.edu.cn
Jinbo Bai
jinbo.bai@centralesupelec.fr

Specialty section:
This article was submitted to Electrochemistry, a section of the journal Frontiers in Chemistry

Received: *30 May 2019*
Accepted: *12 August 2019*
Published: *04 September 2019*

Citation:
Jiang H, Sun W, Li W, Wang Z, Zhou X, Wu Z and Bai J (2019) Facile Synthesis of Novel $V_{0.13}Mo_{0.87}O_{2.935}$ Nanowires With High-Rate Supercapacitive Performance. Front. Chem. 7:595. doi: 10.3389/fchem.2019.00595

INTRODUCTION

Due to overconsumption of non-renewable resources and the growing threat of global warming, reliable and clean energy supplies, such as the secondary battery and supercapacitor (SC) science and technology, are in urgent need of a breakthrough (Liu et al., 2016; Salanne et al., 2016; Liu M. et al., 2018; Liang et al., 2019). SCs are becoming more appealing than ever because of their rapid recharge capabilities, high power density, and durable life cycles (Salanne et al., 2016; Du et al., 2018; Kirubasankar et al., 2018; Ho and Lin, 2019; Le et al., 2019; Ma et al., 2019; Yang L. et al., 2019). It is well-established that three main electrode materials include conducting polymer, transition metal oxide, and carbon materials (Jabeen et al., 2016a,b; Chen et al., 2017; Li et al., 2018; Idrees et al., 2019). In this regard, transition metal oxides can increase the efficiency and improve the specific capacitances compared to conducting polymers and carbon materials (Yang et al., 2015; Fu et al., 2016; Qin et al., 2016a,b; Meng et al., 2017; An and Cheng, 2018). Unfortunately, it has either insufficient electrochemical stability or low conductivity, which still greatly hampers their widespread applications in SCs (Jiang et al., 2012). Therefore, an innovative material that can be applied as a significant electrode material in the field of SCs is still needed.

In the last few years, binary metal oxides with stoichiometric or even nonstoichiometric composition such as $NiCo_2O_4$ (Ma et al., 2016), $NiFe_2O_4$ (Yu et al., 2014), and $MnCo_2O_{4.5}$ (Hu et al., 2019) have achieved efficient energy storage. It stems from its defect–effect mechanisms (Ellis et al., 2007; Wang et al., 2017) or possible jump processes (Hu et al., 2012; Li et al., 2018; Yang Y. et al., 2019) that provided the needed efficient electron conductivity. Also, the electrochemical

behavior of these binary metal oxides is different to simple metal oxides attributed to their composition, including the species and ratios of elements. In particular, binary metal oxides based on molybdenum oxides or vanadium oxides are also regarded as a potential candidate for SCs. Many binary metals–molybdenum oxides, such as $NiMoO_4$ (Cheng et al., 2015), a-$MnMoO_4$ (Purushothaman et al., 2012), $CoMoO_4 \bullet 0.9H_2O$ (Liu et al., 2014), and $NiMoO_4$ (Mehrez et al., 2019), and binary metal–vanadium oxides, such as β-$Na_{0.33}V_2O_5$ (Hong Trang et al., 2014), Li_3VO_4 (Iwama et al., 2016), and $BiVO_4$ (Patil et al., 2016; Guo et al., 2019), have been prepared for high-performance SCs. Despite the tremendous efforts that have been made on the electrode materials for these binary metal oxides, researchers continue to explore the performance of the electrode material for sustainable, low-cost, and clean energy storage and conversion technologies. Especially, binary metal oxides composed of molybdenum–vanadium oxide are also expected to be of favorable potential as SCs. However, such reports are rare.

Herein, we report a simple preparation of one-dimensional $V_{0.13}Mo_{0.87}O_{2.935}$ nanowires through a one-step hydrothermal method. This nanowire electrode exhibits a high specific capacitance of 394.6 F g^{-1} (1 mV s^{-1}) as an electrode material in SC. Additionally, this electrode showed a rate capability of 91.5% (2 to 10 A g^{-1}) and an outstanding cycle stability (97.6% after 10,000 cycles). Therefore, one-dimensional $V_{0.13}Mo_{0.87}O_{2.935}$ nanowires have been prepared and applied as a high-performance SC electrode material.

EXPERIMENTAL

Preparation

Firstly, the molybdenum powder (Mo, 0.192 g, 2 mmol) was mixed with 37 ml of deionized H_2O and 3 ml of hydrogen peroxide at room temperature and then continuous stirred till the solution became light yellow. After that, 0.088 g of ammonium vanadate (NH_4VO_3, 0.75 mmol) was added to the solution until the solid powder was completely dissolved. Then, the resulting solution was decanted into a Teflon reaction kettle and heated in oven at 200°C for 48 h. After cooling to room temperature, the obtained crude products were treated with 2 M nitric acid. Finally, the nanowires were collected through washing with distilled H_2O till neutral and then dried under air at 60°C for 18 h.

Material Characterizations

The X-ray diffractometer (XRD; with Cu-Kα radiation) presented the structure and phase of one-dimensional $V_{0.13}Mo_{0.87}O_{2.935}$ nanowires. The nanowires' morphological feature was studied by a scanning electron microscope (SEM; S-4800) and a transmission electron microscope (TEM; JEM-2100F). Compositions of the samples were tested by X-ray photoelectron spectroscopy (Thermo ESCALAB 250XI). An automated nitrogen adsorption analyzer (ASAP 2020, Micromeritics, America) presented N_2 adsorption–desorption isotherm under the 77 K conditions.

Electrochemical Characterizations

Electrochemistry performances were tested in three electrode systems with 1 M Na_2SO_4 electrolyte using Autolab potentiostat (PGSTAT302N). A saturated calomel electrode (SCE) was used as the reference electrode and a platinum (Pt) foil was used as the counter electrode. The working electrode was a mixture of one-dimensional $V_{0.13}Mo_{0.87}O_{2.935}$ nanowires, acetylene black, and polyvinylidene fluoride (PVDF) according to a certain mass ratio (80:15:5) in a few *N*-methyl pyrrolidinone (NMP). After the mixture was stirred for 24 h, the formed slurry was dripped on graphite paper and then vacuum dried at 60°C for 15 h. Cyclic voltammetry (CV) measurement was carried out in a voltage range of 0–1.0 V at different sweeping rates (1, 5, 10, 25, 50, 75, and 100 mV s^{-1}), and galvanostatic charge–discharge (GCD) was tested at different current densities (2, 4, 6, 8, and 10 A g^{-1}). EIS data are obtained at a frequency from 10^{-2} to 10^5 Hz with an AC amplitude of 5 mV.

RESULTS AND DISCUSSIONS

In the present work, the phase for one-dimensional $V_{0.13}Mo_{0.87}O_{2.935}$ nanowire was first characterized. The XRD spectrum for the prepared product is indicated in **Figure 1** in that all diffraction peaks matched a hexagonal phase of one-dimensional $V_{0.13}Mo_{0.87}O_{2.935}$ nanowires (JCPDS card No. 48-0766). No characteristic peaks from impurity have been detected, suggesting that the pure one-dimensional $V_{0.13}Mo_{0.87}O_{2.935}$ nanowires were prepared. Furthermore, the diffraction peaks were sharp and intense, showing their high degree of crystallinity.

The SEM image in **Figure 2a** depicts the typical morphology of the one-dimensional $V_{0.13}Mo_{0.87}O_{2.935}$ nanowires, which consists of a number of uniform nanowires with an edge length of more than 10 μm. For more detail, the samples were examined by TEM as indicated in **Figure 2b** in that the diameters of the

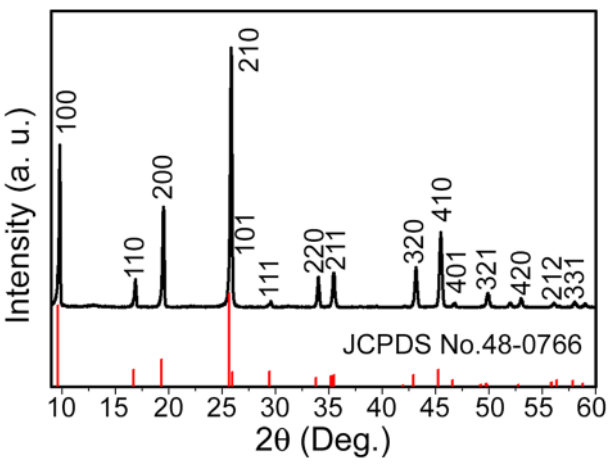

FIGURE 1 | XRD spectrum of the one-dimensional $V_{0.13}Mo_{0.87}O_{2.935}$ nanowires.

nanowires are 20–30 nm with uniform nanostructures. The HR-TEM image is indicated in **Figure 2c**; those one-dimensional $V_{0.13}Mo_{0.87}O_{2.935}$ nanowires have a similar crystal structure and no amorphous phase on the surface. It could be deduced from the lattice fringes that the lattice spacing is 0.26 nm, agreeing to the (220) plane of one-dimensional $V_{0.13}Mo_{0.87}O_{2.935}$ nanowires. In further studying the details, the brighter spots in the FFT pattern (illustration in **Figure 2c**) pointed out an excellent crystal. Besides, **Figure 2d** confirmed that the lattice spacing of 0.26 nm in **Figure 2c** belongs to the (220) plane. These results closely matched the data obtained from the XRD analysis, further confirming the crystal structure of $V_{0.13}Mo_{0.87}O_{2.935}$ nanowires.

The X-ray photoelectron spectroscopy (XPS) shows that the one-dimensional $V_{0.13}Mo_{0.87}O_{2.935}$ nanowires are composed of three elements: V, Mo, and O (**Figure S1** of the Supporting Information). The XPS peak of V 2p in **Figure 3A** was determined to be a peak of V $2p_{3/2}$ of 517.1 eV, and the V $2p_{1/2}$ peak of V^{5+} was not included because the low mole percentage of vanadium in the compound was the smallest (Geert et al., 2004; Liu X. et al., 2018). **Figure 3B** shows the Mo 3d spectrum composed of two peaks, the Mo $3d_{3/2}$ from the peak at 236.0 eV indicates Mo^{6+}, and another peak at 232.9 eV could be due to the superposition of Mo $3d_{5/2}$ and Mo $3d_{3/2}$, which indicates Mo^{6+} and Mo^{5+} (Bica de Moraes et al., 2004). Meanwhile, in **Figure 3C**, the XPS peak of the O 1s was observed at 530.8 eV. In addition, the existence of Mo^{5+} was ascribed to the oxygen anion vacancy in the framework of the compound structure, so that molybdenum is only coordinated by five oxygen species.

The one-dimensional $V_{0.13}Mo_{0.87}O_{2.935}$ nanowires were further investigated by the N_2 adsorption–desorption isotherms

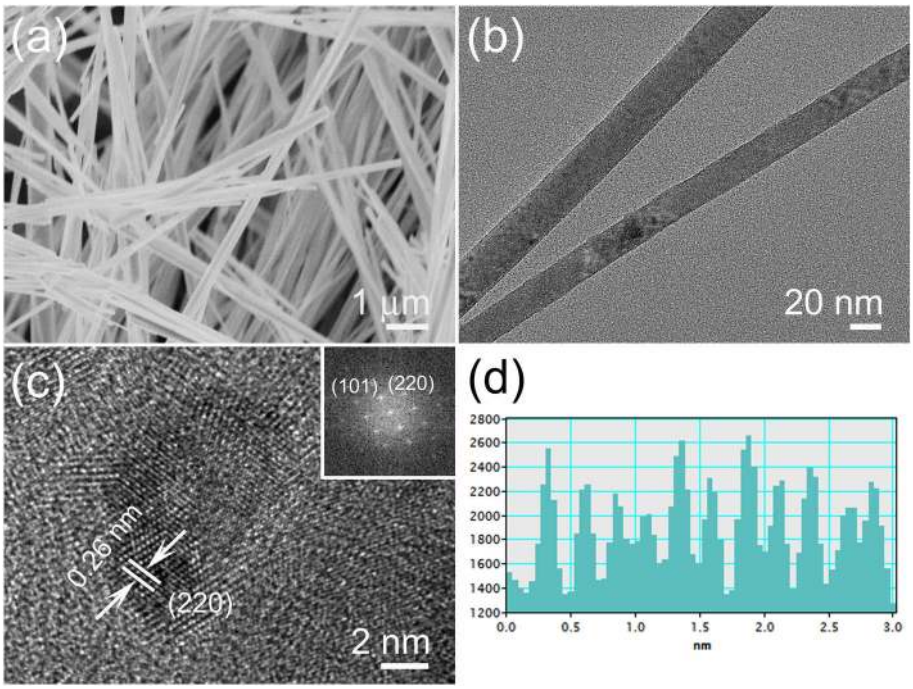

FIGURE 2 | (a) SEM, **(b)** TEM, and **(c)** HR-TEM images of the one-dimensional $V_{0.13}Mo_{0.87}O_{2.935}$ nanowires; the illustration shows the FFT pattern and **(d)** the corresponding lattice spacing obtained from **(c)**.

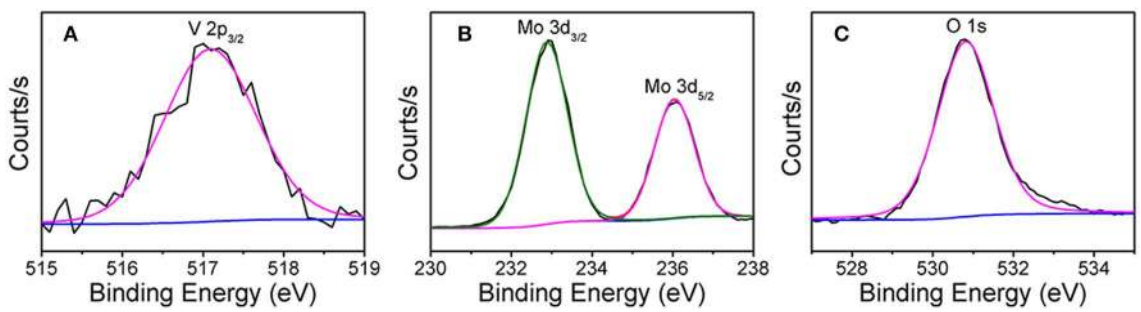

FIGURE 3 | XPS spectra of **(A)** V 2p, **(B)** Mo 3d, and **(C)** O 1s electrons in $V_{0.13}Mo_{0.87}O_{2.935}$ nanowires.

as indicated in **Figure 4**. According to IUPAC, the N_2 adsorption–desorption isotherms of the $V_{0.13}Mo_{0.87}O_{2.935}$ nanowires are a typical type IV adsorption isotherm with the H3 hysteresis loop, exhibiting a mesoporous structure with slit-shaped pores. The BET-specific surface area and pore diameters (illustration in **Figure 4**) of the $V_{0.13}Mo_{0.87}O_{2.935}$ nanowires are about 54.2 m^2 g^{-1} and 80 nm, respectively, which may be attributed to the assembly of the nanowires in space. This porous structure contributes to the diffusion of electrolyte ions and transport during the charge and discharge process of the SC electrodes (Hou et al., 2018, 2019).

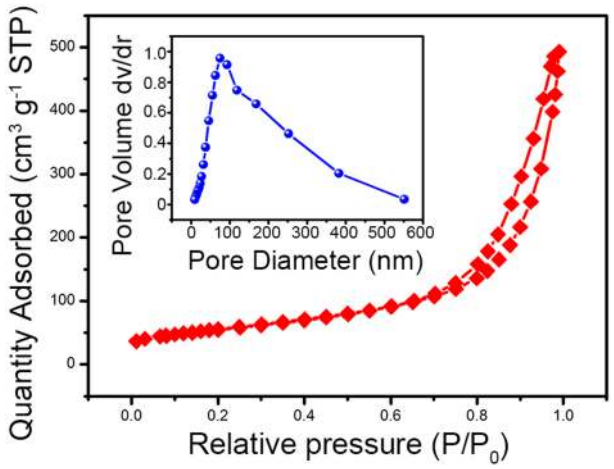

FIGURE 4 | The N_2 adsorption–desorption isotherm and pore size distributions (illustration) of the one-dimensional $V_{0.13}Mo_{0.87}O_{2.935}$ nanowires.

The as-prepared one-dimensional $V_{0.13}Mo_{0.87}O_{2.935}$ nanowires were applied to SC electrode materials. **Figure 5A** depicts the CV curves tested in the voltage from 0 to 1.0 V. Approximate rectangle-shaped and symmetrical CV curves were viewed without redox peaks, showing an EDLC-dominated capacitance behavior of the one-dimensional $V_{0.13}Mo_{0.87}O_{2.935}$ nanowires (Hung et al., 2011; Lokhande et al., 2011; Pujari et al., 2016). Besides, the specific capacitance (**Table S1** of the Supporting Information) of one-dimensional $V_{0.13}Mo_{0.87}O_{2.935}$ nanowires was very high and was 394.6 F g^{-1} at 1 mV s^{-1}. Notably, it can be seen that the CV curve mostly remains in an approximately rectangle-like shape with a sweeping rate between 1 and 100 mV s^{-1}, which confirmed good electrochemical reversibility and outstanding high-energy storage performance; the CV plot tilt increases with increasing scan rates owing to the fact that the electrons do not migrate from the inside of the material to the surface of the electrode in time. **Figure 5B** shows the GCD curves of the one-dimensional $V_{0.13}Mo_{0.87}O_{2.935}$ nanowire electrode at different current densities. It displayed

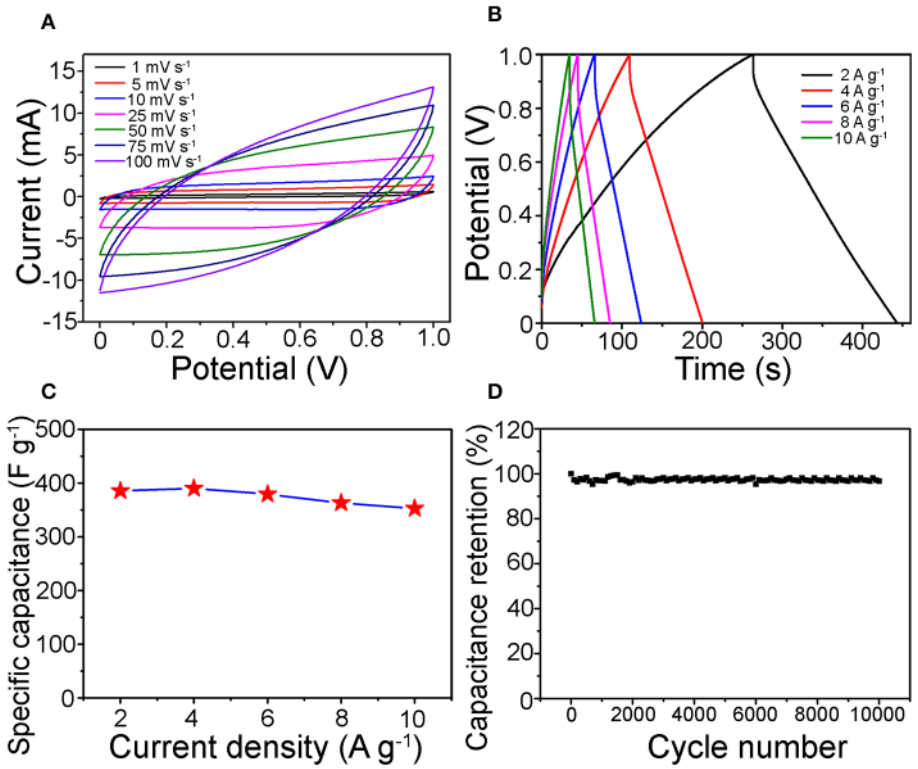

FIGURE 5 | (A) CV and **(B)** GCD curves of the one-dimensional $V_{0.13}Mo_{0.87}O_{2.935}$ nanowire electrodes on different sweeping rates and current densities, respectively. **(C)** Rate performance and **(D)** cycle stability of the $V_{0.13}Mo_{0.87}O_{2.935}$ nanowire electrodes, in 1 M Na_2SO_4 electrolyte.

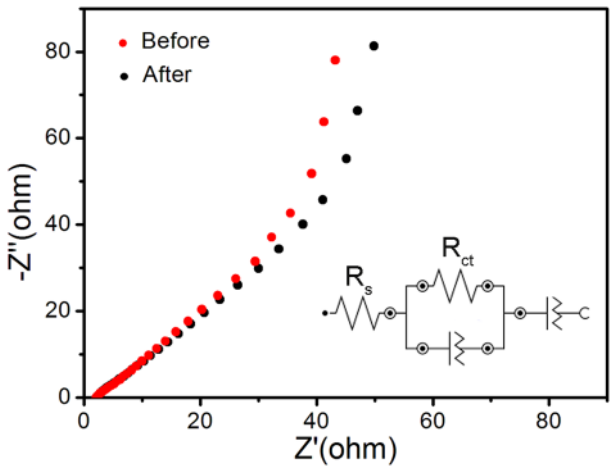

FIGURE 6 | Nyquist plot before and after 10,000 cycles of the one-dimensional $V_{0.13}Mo_{0.87}O_{2.935}$ nanowire electrodes, with the inset showing the corresponding equivalent circuit.

proximate central symmetry voltage profiles, which were consistent compared to the CV results, pointing to the one-dimensional $V_{0.13}Mo_{0.87}O_{2.935}$ nanowires having an excellent reversibility across the whole potential region. Furthermore, one-dimensional $V_{0.13}Mo_{0.87}O_{2.935}$ nanowire electrodes presented high specific capacitances from 385.2 to 352.5 F g^{-1} while discharge current density was enhanced to 2, 4, 6, 8, and 10 A g^{-1} (**Table S2** of the Supporting Information). Compared with other binary metal oxide electrodes, one-dimensional $V_{0.13}Mo_{0.87}O_{2.935}$ nanowire electrodes also indicated a strengthened specific capacitance as reported in the literature, such as $CoMoO_4$ (384 F g^{-1}) (Li et al., 2018), $BiVO_4$ (116.3 F g^{-1}) (Patil et al., 2016), and $MnMoO_4$ (168.32 F g^{-1}) (Veerasubramani et al., 2014).

The specific capacitances of the $V_{0.13}Mo_{0.87}O_{2.935}$ electrodes with different current densities are indicated in **Figure 5C**. It maintained a remarkable rate performance of 91.5% from 2 to 10 A g^{-1}. This result may be attributed to the active materials to form porous channels through intertwined networks, enabling efficient electrolyte transport and accessibility of active sites (Jiang et al., 2011). Therefore, it is possible to maintain a high specific capacitance even at higher current densities. **Figure 5D** indicates the long-term cycle stability of the one-dimensional $V_{0.13}Mo_{0.87}O_{2.935}$ nanowire electrode, which was tested through CV tests repeating 10,000 cycles at 50 mV s^{-1}. It can be observed that its specific capacitance retention showed outstanding stability, with the increase in some cycles fluctuating only a little. After 10,000 cycles, the retention rate value was found to be 97.6% of the initial value.

The $V_{0.13}Mo_{0.87}O_{2.935}$ electrodes were subjected to electrochemical impedance spectroscopy (EIS) to explore relevant charge transfer resistance. **Figure 6** shows the Nyquist plot before and after 10,000 cycles of the one-dimensional $V_{0.13}Mo_{0.87}O_{2.935}$ nanowire electrodes. The inset shows the corresponding equivalent circuit by its corresponding fitting curve (**Figure S2** in Supporting Information), which was fitted by an equivalent circuit consisting of a bulk solution resistance R_s, a charge-transfer R_{ct}, and constant phase element (CPE). The R_s values of the one-dimensional $V_{0.13}Mo_{0.87}O_{2.935}$ nanowire electrode before and after 10,000 cycles are 2.02 and 2.10 Ω, respectively. Also, the value of R_{ct} was connected with charge transfer after 10,000 cycles and is only slightly higher than before (68.6 vs. 50.1 Ω), manifesting superior conductivity and stability of the one-dimensional $V_{0.13}Mo_{0.87}O_{2.935}$ nanowire microstructure owing to good ion conductivity of the interface between electrolyte and electrodes.

CONCLUSIONS

In summary, one-dimensional $V_{0.13}Mo_{0.87}O_{2.935}$ nanowires were synthesized under a facile one-step hydrothermal condition. For application in a SC electrode, it was found to present a high specific capacitance of 394.6 F g^{-1} (1 mV s^{-1}). Besides, this electrode showed a perfect rate capability of 91.5% at the current density that was enhanced five times and outstanding long-term cyclic stability (97.6% after 10,000 cycles). This study offers a common preparation method of binary molybdenum–vanadium oxide used in SCs with a superior electrochemical property.

DATA AVAILABILITY

All datasets generated for this study are included in the manuscript/**Supplementary Files**.

AUTHOR CONTRIBUTIONS

WL conceived and designed the experiments. HJ, WS, and ZWa performed the experiments and analyzed the data. HJ and WS wrote and revised the manuscript. WL, ZWu, XZ, and JB discussed and supervised the whole project. All the authors revised and checked draft.

FUNDING

The research was supported by the National Natural Science Foundation of China (51602193), Shanghai Chen Guang project (16CG63), the Fundamental Research Funds for the Central Universities (WD1817002) and the Talent Program of Shanghai University of Engineering Science, the Natural Science Foundation of Shandong Province of China (ZR2019BB002), and Shanghai University of Engineering Science Innovation Fund (18KY0503).

SUPPLEMENTARY MATERIAL

The Supplementary Material for this article can be found online at: https://www.frontiersin.org/articles/10.3389/fchem.2019.00595/full#supplementary-material

REFERENCES

An, T., and Cheng, W. (2018). Recent progress in stretchable supercapacitors. *J. Mater. Chem. A* 6, 15478–15494. doi: 10.1039/C8TA03988G

Bica de Moraes, M. A., Trasferetti, B. C., Rouxinol, F. P., Landers, R., Durrant, S. F., Scarmínio, J., et al. (2004). Molybdenum oxide thin films obtained by the hot-filament metal oxide deposition technique. *Chem. Mater.* 16, 513–520. doi: 10.1021/cm034551a

Chen, X., Paul, R., and Dai, L. (2017). Carbon-based supercapacitors for efficient energy storage. *Natl. Sci. Rev.* 4, 453–489. doi: 10.1093/nsr/nwx009

Cheng, D., Yang, Y., Xie, J., Fang, C., Zhang, G., and Xiong, J. (2015). Hierarchical $NiCo_2O_4$ @$NiWO_4$ core-shell hybrid nanowire/nanosheet arrays for high-performance pseudocapacitors. *J. Mater. Chem. A* 3, 14348–14357. doi: 10.1039/C5TA03455H

Du, W., Wang, X., Zhan, J., Sun, X., Kang, L., Jiang, F., et al. (2018). Biological cell template synthesis of nitrogen-doped porous hollow carbon spheres/MnO_2 composites for high-performance asymmetric supercapacitors. *Electrochim. Acta* 296, 907–915. doi: 10.1016/j.electacta.2018.11.074

Ellis, B., Subramanya Herle, P., Rho, Y.-H., Nazar, L. F., Dunlap, R., Perry, L. K., et al. (2007). Nanostructured materials for lithium-ion batteries: surface conductivity vs. bulk ion/electron transport. *Faraday Discuss.* 134, 119–141. doi: 10.1039/B602698B

Fu, W., Wang, Y., Han, W., Zhang, Z., Zha, H., and Xie, E. (2016). Construction of hierarchical $ZnCo_2O_4$@Ni_xCo_{2x} $(OH)_{6x}$ core/shell nanowire arrays for high-performance supercapacitors. *J. Mater. Chem. A* 4, 173–182. doi: 10.1039/C5TA07965A

Geert, S., Depla, D., Poelman, H., Marin, G. B., and De Gryse, R. (2004). Determination of the V2p XPS binding energies for different vanadium oxidation states (V^{5+} to V^{0+}). *J. Electron Spectrosc. Relat. Phenom.* 135, 167–175. doi: 10.1016/j.elspec.2004.03.004

Guo, Z., Li, R., Zhu, X., Fu, Q., Liang, G., Chen, Y., et al. (2019). Nanosheet-based $Nb_{12}O_{29}$ hierarchical microspheres for enhanced lithium storage. *Chem. Commun.* 55, 2493–2496. doi: 10.1039/C8CC09924C

Ho, K.-C., and Lin, L.-Y. (2019). A review of electrode materials based on core–shell nanostructures for electrochemical supercapacitors. *J. Mater. Chem. A* 7, 3516–3530. doi: 10.1039/C8TA11599K

Hong Trang, N. T., Lingappan, N., Shakir, I., and Kang, D. J. (2014). Growth of single-crystalline β-$Na_{0.33}V_2O_5$ nanowires on conducting substrate: a binder-free electrode for energy storage devices. *J. Power Sources* 251, 237–242. doi: 10.1016/j.jpowsour.2013.11.041

Hou, C., Tai, Z., Zhao, L., Zhai, Y., Hou, Y., Fan, Y., et al. (2018). High performance MnO@C microcages with a hierarchical structure and tunable carbon shell for efficient and durable lithium storage. *J. Mat. Chem. A* 6, 9723–9736. doi: 10.1039/C8TA02863J

Hou, C., Wang, J., Du, W., Wang, J., Du, Y., Liu, C., et al. (2019). One-pot synthesized molybdenum dioxide–molybdenum carbide heterostructures coupled with 3D holey carbon nanosheets for highly efficient and ultrastable cycling lithium-ion storage. *J. Mat. Chem. A* 7, 13460–13472. doi: 10.1039/C9TA03551F

Hu, L., Wu, L., Liao, M., Hu, X., and Fang, X. (2012). Electrical transport properties of large, individual $NiCo_2O_4$ nanoplates. *Adv. Funct. Mater.* 22, 998–1004. doi: 10.1002/adfm.201102155

Hu, X., Nan, H., Liu, M., Liu, S., An, T., and Tian, H. (2019). Battery-like $MnCo_2O_4$ electrode materials combined with active carbon for hybrid supercapacitors. *Electrochim. Acta* 306, 599–609. doi: 10.1016/j.electacta.2019.03.166

Hung, C., Hung, J., Lin, P., and Tseng, T. (2011). Electrophoretic fabrication and characterizations of manganese oxide/carbon nanotube nanocomposite pseudocapacitors. *J. Electrochem. Soc.* 158, A942–A947. doi: 10.1149/1.3601862

Idrees, M., Batool, S., Kong, J., Zhuang, Q., Liu, H., Shao, Q., et al. (2019). Polyborosilazane derived ceramics—Nitrogen sulfur dual doped graphene nanocomposite anode for enhanced lithium ion batteries. *Electrochim. Acta* 296, 925–937. doi: 10.1016/j.electacta.2018.11.088

Iwama, E., Kawabata, N., Nishio, N., Kisu, K., Miyamoto, J., Naoi, W., et al. (2016). Enhanced electrochemical performance of ultracentrifugation-derived nc-Li_3VO_4/MWCNT composites for hybrid supercapacitors. *ACS Nano* 10, 5398–5404. doi: 10.1021/acsnano.6b01617

Jabeen, N., Xia, Q., Savilov, S. V., Aldoshin, S. M., Yu, Y., and Xia, H. (2016a). Enhanced pseudocapacitive performance of α-MnO_2 by cation preinsertion. *ACS Appl. Mater. Inter.* 8, 33732–33740. doi: 10.1021/acsami.6b12518

Jabeen, N., Xia, Q., Yang, M., and Xia, H. (2016b). Unique core–shell nanorod arrays with polyaniline deposited into mesoporous $NiCo_2O_4$ support for high-performance supercapacitor electrodes. *ACS Appl. Mater. Inter.* 8, 6093–6100. doi: 10.1021/acsami.6b00207

Jiang, H., Zhao, T., Ma, J., Yan, C., and Li, C. (2011). Ultrafine manganese dioxidenanowire network for high-performance supercapacitors. *Chem. Commun.* 47, 1264–1266. doi: 10.1039/C0CC04134C

Jiang, J., Li, Y., Liu, J., Huang, X., Yuan, C., and Lou, X. W. (2012). Recent advances in metal oxide-based electrode architecture design for electrochemical energy storage. *Adv. Mater.* 24, 5166–5180. doi: 10.1002/adma.201202146

Kirubasankar, B., Murugadoss, V., Lin, J., Ding, T., Dong, M., Liu, H., et al. (2018). *In situ*, grown nickel selenide on graphene nanohybrid electrodes for high energy density asymmetric supercapacitors. *Nanoscale* 10, 20414–20425. doi: 10.1039/C8NR06345A

Le, K., Wang, Z., Wang, F., Wang, Q., Shao, Q., Murugadoss, V., et al. (2019). Sandwich-like NiCo layered double hydroxides/reduced graphene oxide nanocomposite cathode for high energy density asymmetric supercapacitors. *Dalton Transact.* 175, 16–20. doi: 10.1039/C9DT00615J

Li, W., Wang, X., Hu, Y., Sun, L., Gao, C., Zhang, C., et al. (2018). Hydrothermal synthesized of $CoMoO_4$ microspheres as excellent electrode material for supercapacitor. *Nanoscale Res. Lett.* 13:120. doi: 10.1186/s11671-018-2540-3

Liang, C., Li, C., He, Y., Li, G., Yu, Y., Lou, Y., et al. (2019). Use of hyperaccumulator to enrich metal ions for supercapacitor. *Adv. Electron. Mater.* 5:1900094. doi: 10.1002/aelm.201900094

Liu, M., Meng, Q., Yang, Z., Zhao, X., and Liu, T. (2018). Ultra-long-term cycling stability of an integrated carbon–sulfur membrane with dual shuttle-inhibiting layers of graphene "nets" and a porous carbon skin. *Chem. Commun.* 54, 5090–5093. doi: 10.1039/C8CC01889H

Liu, M., Yang, Z., Sun, H., Lai, C., Zhao, X., Peng, H., et al. (2016). A hybrid carbon aerogel with both aligned and interconnected pores as interlayer for high-performance lithium–sulfur batteries. *Nano Res.* 9, 3735–3746. doi: 10.1007/s12274-016-1244-1

Liu, M.-C., Kong, L.-B., Kang, L., Li, X., Walsh, F. C., Xing, M., et al. (2014). Synthesis and characterization of $M_3V_2O_8$ (M = Ni or Co) based nanostructures: a new family of high performance pseudocapacitive materials. *J. Mater. Chem. A* 2, 4919–4926. doi: 10.1039/c4ta00582a

Liu, X., Wang, J., and Yang, G. (2018). *In situ* growth of the $Ni_3V_2O_8$@PANI composite electrode for flexible and transparent symmetric supercapacitors. *ACS Appl. Mater. Inter.* 10, 20688–20695. doi: 10.1021/acsami.8b04609

Lokhande, C., Dubal, D., and Joo, O. (2011). Metal oxide thin film based supercapacitors. *Curr. Appl. Phys.* 11, 255–270. doi: 10.1016/j.cap.2010.12.001

Ma, F.-X., Yu, L., Xu, C.-Y., and Lou, X. W. (David). (2016). Self-supported formation of hierarchical NiCo2O4 tetragonal microtubes with enhanced electrochemical properties. *Energy Environ. Sci.* 9, 862–866. doi: 10.1039/C5EE03772G

Ma, Y., Hou, C., Zhang, H., Zhang, Q., Liu, H., and Wu, S. (2019). Three-dimensional core–shell Fe_3O_4/polyaniline coaxial heterogeneous nanonets: preparation and high performance supercapacitor electrodes. *Electrochim. Acta* 315, 114–123. doi: 10.1016/j.electacta.2019.05.073

Mehrez, J. A.-A., Owusu, K. A., Chen, Q., Li, L., Hamwi, K., Luo, W., et al. (2019). Hierarchical $MnCo_2O_4$@$NiMoO_4$ as free-standing core–shell nanowire arrays with synergistic effect for enhanced supercapacitor performance. *Inorg. Chem. Front.* 6, 857–865. doi: 10.1039/C8QI01420E

Meng, Q., Cai, K., Chen, Y., and Chen, L. (2017). Research progress on conducting polymer based supercapacitor electrode materials. *Nano Energy* 36, 268–285. doi: 10.1016/j.nanoen.2017.04.040

Patil, S. S., Dubal, D. P., Deonikar, V. G., Tamboli, M. S., Ambekar, J. D., Gomez-Romero, P., et al. (2016). Fern-like rGO/$BiVO_4$ hybrid nanostructures for high-energy symmetric supercapacitor. *ACS Appl. Mater. Inter.* 8, 31602–31610. doi: 10.1021/acsami.6b08165

Pujari, R., Lokhande, V., Kumbhar, V., Chodankar, N., and Lokhande, C. (2016). Hexagonal microrods architectured MoO3 thin film for supercapacitor application. *J. Mater. Sci.* 27, 3312–3317. doi: 10.1007/s10854-015-4160-3

Purushothaman, K. K., Cuba, M., and Muralidharan, G. (2012). Supercapacitor behavior of α-$MnMoO_4$ nanorods on different electrolytes. *Mater. Res. Bull.* 47, 3348–3351. doi: 10.1016/j.materresbull.2012.07.027

Qin, T., Liu, B., Wen, Y., Wang, Z., Jiang, X., Wan, Z., et al. (2016a). Freestanding flexible graphene foams@polypyrrole@MnO_2 electrodes for high-performance supercapacitors. *J. Mater. Chem. A* 4, 9196–9203. doi: 10.1039/C6TA02835G

Qin, T., Wan, Z., Wang, Z., Wen, Y., Liu, M., Peng, S., et al. (2016b). 3D flexible O/N Co-doped graphene foams for supercapacitor electrodes with high volumetric and areal capacitances. *J. Power Sources* 336, 455–464. doi: 10.1016/j.jpowsour.2016.11.003

Salanne, M., Rotenberg, B., Naoi, K., Kaneko, K., Taberna, P.-L., Grey, C. P., et al. (2016). Efficient storage mechanisms for building better supercapacitors. *Nat. Energy* 1:16070. doi: 10.1038/nenergy.2016.70

Veerasubramani, G. K., Krishnamoorthy, K., Sivaprakasam, R., and Kim, S. J. (2014). Sonochemical synthesis, characterization, and electrochemical properties of $MnMoO_4$ nanorods for supercapacitor applications. *Mater. Chem. Phys.* 147, 836–842. doi: 10.1016/j.matchemphys.2014.06.028

Wang, G., Yang, Y., Han, D., and Li, Y. (2017). Oxygen defective metal oxides for energy conversion and storage. *Nano Today* 13, 23–39. doi: 10.1016/j.nantod.2017.02.009

Yang, J., Yu, C., Fan, X., Zhao, C., and Qiu, J. (2015). Ultrafast self-assembly of graphene oxide-induced monolithic NiCo-carbonate hydroxide nanowire architectures with a superior volumetric capacitance for supercapacitors. *Adv. Funct. Mater.* 25, 2109–2116. doi: 10.1002/adfm.201404019

Yang, L., Shi, M., Jaing, J., Liu, Y., Yang, C., Liu, H., et al. (2019). Heterogeneous interface induced formation of balsam pear-like PPy for high performance supercapacitors. *Mater. Lett.* 244, 27–30. doi: 10.1016/j.matlet.2019.02.064

Yang, Y., Li, S., Huang, W., Shangguan, H., Engelbrekt, C., Duan, S., et al. (2019). Effective synthetic strategy of $Zn_{0.76}Co_{0.24}S$ encapsulated in stabilized N-doped carbon nanoarchitecture toward ultra-long-life hybrid supercapacitors. *J. Mat. Chem. A* 7, 14670–14680. doi: 10.1039/C9TA03575C

Yu, Z.-Y., Chen, L.-F., and Yu, S.-H. (2014). Growth of NiFe2O4 nanoparticles on carbon cloth for high performance flexible supercapacitors. *J. Mater. Chem. A* 2, 10889–10894. doi: 10.1039/c4ta00492b

Conflict of Interest Statement: The authors declare that the research was conducted in the absence of any commercial or financial relationships that could be construed as a potential conflict of interest.